Department of Engineering Physics and Mathematics
Helsinki University of Technology
Espoo, Finland

MONTE CARLO SIMULATION OF CHARGED PARTICLE ORBITS IN THE PRESENCE OF RADIOFREQUENCY WAVES IN TOKAMAK PLASMAS

Seppo Sipilä

Espoo 1997

Department of Engineering Physics and Mathematics
Helsinki University of Technology
Espoo, Finland

MONTE CARLO SIMULATION OF CHARGED PARTICLE ORBITS IN THE PRESENCE OF RADIOFREQUENCY WAVES IN TOKAMAK PLASMAS

Seppo Sipilä

Dissertation for the degree of Doctor of Technology to be presented with due permission for public examination and debate in Auditorium J at Helsinki University of Technology (Espoo, Finland) on the 15th of December, 1997, at 12 o'clock noon.

Espoo 1997

Abstract

A review of tracking charged particle motion in an axisymmetric toroidal plasma and of Monte Carlo modelling of particle–background interactions is given. Computational methods for efficient modelling of electron and ion guiding center orbits in tokamaks are described and the Monte Carlo orbit-following code ASCOT is reviewed. The efficiency of the code is based on the use of a coordinate system specifically designed for a toroidal system, on preventing numerical error accumulation, and on accelerating interaction time scales. Solutions for enhancing the computational efficiency of the Monte Carlo operators without deterioration of accuracy are described. Applications of the ASCOT code to studies of reverse runaway electrons, lower hybrid (LH) and ion cyclotron (IC) heating and current drive are presented.

Relativistic effects are found to increase the reverse runaway probability of fast electrons during current ramp-up. Collisions, acting to diminish the total energy of the electrons towards thermal energy, have a lesser effect on the velocity of the test electron at relativistic energies. Combined to the effect of pitch collisions which bring the electrons towards the trapping cone (where they can traverse a wide region in velocity parallel to the magnetic field ($v_{||}$) on a fast time scale on their way to the reverse runaway velocity region), this relativistic effect enables the electrons to reach the trapping cone at a large total velocity, where the trapping cone is wide and the $v_{||}$ region traversed during trapped orbit motion is larger. This brings forth a notable increase in the reverse runaway probability.

In a realistic tokamak configuration with smooth wave diffusion and fusion reactivity profiles, fusion-born alpha particles are found to interact with lower hybrid waves by absorbing energy from the wave. No wave amplification is observed. Special absorbing boundary conditions must be applied at the perpendicular energy boundary of the wave region in order to reverse the direction of energy transfer.

A parameter study of ion cyclotron heating and current drive indicates that the power efficiency of minority ion current generation by IC waves is optimized for small values of local major radius and for high electron temperatures in the studied parameter range.

ISBN 951-22-3856-X

Preface

This work was carried out at Advanced Energy Systems (formerly Nuclear Engineering Laboratory), Helsinki University of Technology, from 1991 to 1997.

I wish to warmly thank my instructor, Dr. Jukka Heikkinen, for his invaluable guidance and support in the course of this work. The supervisor of my work, Prof. Rainer Salomaa, I thank for his interest and for urging me on to complete this work in a finite amount of time. I am also grateful to all the staff of the laboratory and of VTT Energy for being such nice people to work with.

Financial support from the Academy of Finland, the Imatran Voima Foundation, the Jenny and Antti Wihuri Fund and the Foundation for the Advancement of Science is gratefully acknowledged.

My folks are to thank for their encouragement and enthusiasm, and for making it possible throughout all these years for me to end up like this.

"All work and no play makes Seppo a dull boy". Thanks are due to all my friends for doing their best to prevent this.

My dear wife Outi should be decorated with a medal for bearing with me. Outi, thank you so much for being there. A huge, grateful hug will be delivered to you right after the dissertation.

Espoo, November 1997

Seppo Sipilä

List of publications

This paper is an introduction to the following publications:

I. J.A. Heikkinen, S.K. Sipilä, and T.J.H. Pättikangas, "Monte Carlo Simulation of Runaway Electrons in a Toroidal Geometry", Computer Physics Communications **76** (1993) pp. 215–230.

II. J.A. Heikkinen, S.J. Karttunen, T.J.H. Pättikangas, and S.K. Sipilä, "Runaway Losses in Current Ramp-Up with Lower Hybrid Waves", Nuclear Fusion **33** (1993) pp. 887–894.

III. S.K. Sipilä, and J.A. Heikkinen, "Monte Carlo Simulation of Lower Hybrid Current Drive in Tokamaks", IEEE Transactions on Plasma Science **22** (1994) pp. 260–266.

IV. J.A. Heikkinen and S.K. Sipilä, "Alpha Particle Transport-Driven Current in Tokamaks", Physical Review E **51** (1995) pp. 1655–1658.

V. J.A. Heikkinen and S.K. Sipilä, "Power Transfer and Current Generation of Fast Ions with Large-k_θ Waves in Tokamak Plasmas", Physics of Plasmas **2** (1995) pp. 3724–3733.

VI. J.A. Heikkinen and S.K. Sipilä, "Monte Carlo Simulation of Minority Ion Bootstrap Current by Off-Axis Ion Cyclotron Heating in Tokamaks", Nuclear Fusion **37** (1997) 835–849.

Publications I–II deal with the application of guiding center orbit-following methods to study reverse runaway electrons in a tokamak. **Publication I** gives a description of the ASCOT code and the methods applied in it. Toroidicity and finite temperature effects on the runaway rate are presented. In **Publication II**, these effects are taken into account in a study of the efficiency of plasma current ramp-up by lower hybrid (LH) waves.

Publication III presents a Monte Carlo operator for orbit-following simulation of electron LH current drive in toroidal geometry. The ASCOT code is applied to a study of LH current drive efficiency, and LH–driven current density profiles are presented for wave power deposition profiles of different width with and without anomalous radial diffusion.

Publications IV–V study the transport of fusion-born alpha particles and their interaction with radiofrequency waves in a tokamak. A Monte Carlo operator for ion interaction with LH waves is presented and a mechanism of current

generation by the interaction of fusion-born alpha particles with radially localized LH waves is studied.

In **Publication VI**, a Monte Carlo operator modelling ion cyclotron (IC) heating in orbit-following simulations is applied to a study of minority ion bootstrap current density modifications caused by the IC wave. The effects on the current density are compared with a semianalytical model and the efficiency of current generation is scanned as a function of the electron temperature, the wave electric field, and the major radius and aspect ratio of the tokamak.

The author has actively participated in all work reported in this thesis. He was the principal author of **Publication III**. He has written the ASCOT code and performed all the numerical work to which ASCOT was applied, i.e., all the simulations for **Publications I–III** and most of the numerical work for **Publications IV–VI**.

Contents

1 Introduction

Controlled nuclear fusion is a promising source of energy for the future. By fusing light nuclei together at high temperature and density, substantial amounts of nuclear energy can be released without creating large amounts of long-lived waste products in the process.

At present, one of the most promising method of producing thermonuclear energy is magnetic confinement fusion in tokamaks. The results achieved in various tokamak devices have improved steadily, and the large tokamak experiments such as JET (Joint European Torus, UK) and TFTR (Tokamak Fusion Test Reactor, USA) have demonstrated notable releases of fusion energy in the 90's. The progress made in tokamak confinement has lead to results very close to break–even conditions, where the released fusion energy equals the amount of energy

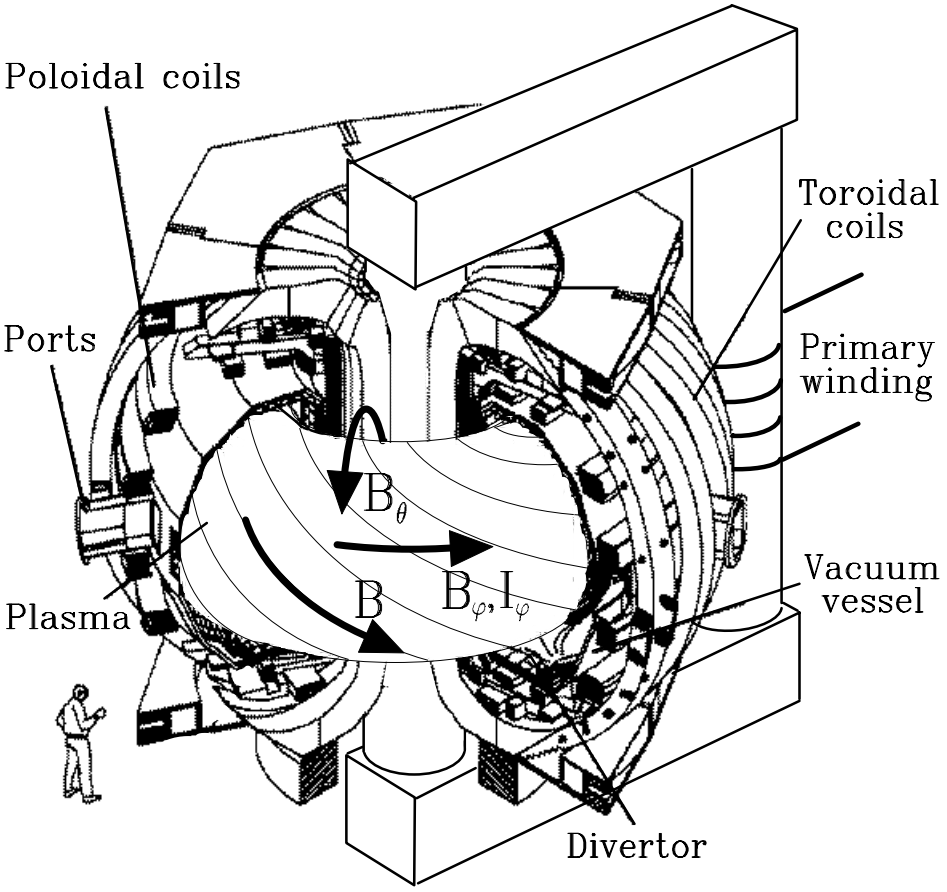

Figure 1: The major components of a tokamak.

applied to heat the plasma.

Tokamak confinement is based on the closed toroidal magnetic configuration in which the magnetic field lines twist helically around the torus (Fig. 1). Gyrating around the magnetic field lines, the charged particles (ions and electrons) that comprise the tokamak plasma are restricted in their motion perpendicular to the magnetic field. However, in addition to this gyromotion and their motion along the field lines, the particles have a drift velocity in the direction perpendicular to the magnetic field and its gradient. The helicity of the magnetic field lines prevents the particles from escaping confinement because of this drift.

The magnetic field isolates the plasma from the walls of the containment vessel. The toroidal magnetic field B_φ, which stabilizes the system, is produced by coils outside the vessel. The strong toroidal current I_φ is usually induced in the plasma by making it act as the secondary winding of a transformer. This current gives rise to a poloidal magnetic field B_θ, which tends to contract the plasma inwards making the toroidal plasma column thinner. Additional coils are used to shape and position the plasma.

The conditions for fusion ignition are easiest to achieve by using a mixture of the two heavier isotopes of hydrogen, deuterium (D) and tritium (T) as fuel. Thus, the first generation of fusion reactors will be based on deuterium–tritium (DT) fusion. The fusion reaction in this case is

$$ {}^{2}_{1}\mathrm{D} + {}^{3}_{1}\mathrm{T} \rightarrow {}^{4}_{2}\mathrm{He} + {}^{1}_{0}\mathrm{n} + 17.6\ \mathrm{MeV}, $$

i.e., a helium nucleus (an alpha particle) and a neutron are produced. The combined kinetic energy of the reaction product particles is 17.6 MeV, with about 3.5 MeV going to the alpha particle and 14.1 MeV to the neutron. The energetic neutron, not confined by the magnetic field, will instantly escape from the plasma and is absorbed in outer structures of the reactor, where it is utilized to breed tritium fuel from lithium. The alpha particle is confined by the magnetic field and will expend its energy in collisions with the plasma particles, thus contributing to the heating of the plasma.

Achieving reactor conditions in a DT plasma requires that the so-called fusion product $n_i \tau_\varepsilon T_i$ must be of the order of 5×10^{21} m^{-3} s keV. Here, n_i and T_i denote the number density and temperature of the plasma and τ_ε is the energy confinement time. A density of about 10^{20} m^{-3} and a temperature of over 100 million °C (10 keV) is thus required when the confinement time is of the order of seconds. Such extreme conditions require efficient heating methods and a good

insulation of the plasma from the vacuum vessel wall. In addition to the ohmic heating caused by the plasma current (up to a plasma temperature of about 3–4 keV), additional heating by radiofrequency (RF) waves or by neutral beam injection (NBI) must be used. In order to achieve continuous operation instead of the pulsed operation of a tokamak with transformer-induced plasma current, methods of generating and driving continuous plasma current with RF waves are being studied.

A good understanding of particle and energy transport by fusion-born alpha particles and RF–heated plasma electrons and ions in a magnetically confined plasma is essential for the design of large scale magnetic confinement experiments of the future. In the theoretical studies of these phenomena, computational plasma physics has become an important tool in the course of the rapid evolution in computer power. Computer simulations are applied to studies of the physics of future confinement devices as well as testing of theoretical models in the light of present experimental results. There are two main approaches to computational plasma physics. In the magnetohydrodynamic (MHD) approach, the macroscopic behaviour of the plasma in the presence of magnetic fields is studied numerically using the MHD equations, presenting the plasma as a fluid. The kinetic approach utilizes more detailed descriptions of the plasma. It is based on solving the kinetic equations of the plasma directly or by using test particle simulations, in which the motion of individual particles in external fields and in the presence of particle interactions is computed.

Generating statistics of the behaviour of a physical system by Monte Carlo simulation [1, 2] is an efficient numerical tool in statistical physics. In plasma physics, this technique is particularly important in calculating the guiding center orbits of high energy particles in complicated geometries in the presence of various particle interactions with the background plasma and electromagnetic waves. In order to evaluate transport coefficients and particle trajectories in toroidal magnetized plasmas, several orbit-following codes, exploiting Monte Carlo operators to model particle–background interactions as needed, have been developed, such as the code of Tani et al. [3], the code of Boozer and Kuo-Petravic [4], the codes ORBIT [5] and ORBITX [6], FAFNER [7], HELIOS [8], HECTOR [9] and others [10]. The orbit-following Monte Carlo (OFMC) techniques are also being used as part of more general transport codes such as TRANSP [11] and particle-in-cell (PIC) codes such as those of the ES1/TESS/DIPSI family [12]. In recent years, OFMC techniques have been adopted to gyrokinetic simulations

of phenomena such as ion temperature gradient driven instabilities [13–17] and neoclassical transport [18].

A wide range of problems have been investigated with orbit-following Monte Carlo methods. Evaluations of orbit losses [19–23], ion thermal conductivity [24] and particle transport [4,25–31] have been made. Ion loss orbits at the edge of a divertor tokamak plasma in the presence of a radial electric field have been studied in detail [32] using the orbit-following approach. Numerous auxiliary heating simulations have also been presented. The effect of ion cyclotron radiofrequency (ICRF) heating on particle confinement in tokamaks has been studied [33–35] as well as the effect of finite orbit widths on the radial power absorption profile [35,36] and on the current density profile of ICRF-heated ions [37,38] (see also **Publication VI**). The effects of finite beta, finite orbit width and a radial electric field on ICRF heating in non-axisymmetric helical devices have been simulated by similar methods [39]. Lower hybrid (LH) wave interaction with energetic ions has been investigated (see **Publications IV–V**).

In addition to ion studies, electron behavior in the presence of RF waves has been simulated using the orbit-following method [40] (see also **Publications I–III**). Other wave-particle phenomena, such as the interaction of toroidal Alfvén Eigenmodes (TAE) and fusion-born alpha particles, have been investigated [41–44] as well. Heating methods not based on RF waves, such as NBI heating, have been studied both in non-axisymmetric devices and axisymmetric tokamak geometry [3,45–49].

The behavior of charged particles in the presence of toroidal magnetic field ripple, being a problem involving intricate particle behavior, has been widely studied using orbit-following techniques. Simulations have been made to study the radial penetration of NBI-injected ions in the presence of a vertically asymmetric toroidal field ripple [50], the ripple losses of NBI or RF heated ions [51,52] as well as ripple losses of fusion-born alpha particles [51,53–56]. Fusion burn control by toroidal magnetic field ripple in non-circular, high-current plasmas has been studied [57] as well as geometry effects on alpha particle ripple loss [58] and the feasibility of ripple-assisted fueling [59]. Machine-specific comparisons to experimental ripple loss results of the JT-60U tokamak have also been made [60–62].

Several variations and refinements of the orbit-following approach have been devised. Calculational efficiency enhancements to ripple loss simulations have been developed, based either on the use of the guiding center orbit approach only

near the ripple trapping/detrapping boundary [63], or on the omission of the ripple component of the magnetic field in parameter regions where it is of little importance [64]. A method of presenting particle orbits by a set of unperturbed orbit invariants and evaluating their changes due to collisions and wave-particle interactions using the Monte Carlo method has been presented [36]. In this method, the drift orbits of the test particles in configuration space need not be followed, which eliminates the need for the numerous time-consuming evaluations of local background quantities related to the equations of motion and thus speeds up the computation. The changes to the invariants are calculated over orbits and accelerated numerically. On the other hand, this method requires tabulation and time-consuming interpolation in the invariant space in more than two dimensions, and numerical acceleration techniques can be applied to the conventional orbit-following approach as well to avoid recalculation of many similar orbits. The conventional orbit-following method is also easily applicable to orbit calculations in the presence of ripple magnetic fields and in divertor geometries, where the application of the invariant method is difficult. In the course of the development work and successful application to a wide variety of problems, the orbit-following Monte Carlo technique has become a well-established approach to problems that require a detailed description of particle trajectories.

This work describes the numerical approach and the applications of the computer code ASCOT (**A**ccelerated **S**imulation of **C**harged Particle **O**rbits in a **T**okamak). Originally developed for the study of electron guiding center orbits, the ASCOT code has eventually been expanded into a versatile tool for both electron and ion studies in tokamak plasmas of noncircular cross section, including actual experimental magnetic field configurations with X-point and divertor plates. This report gives an overview of the various numerical approaches tested and applied and of the problems encountered in the course of developing ASCOT. A summary of the obtained results is also given with an emphasis on the effects revealed by taking relativistic effects into account in electron studies and by studying wave-particle interactions in a realistic toroidal configuration.

Relativistic effects are found to increase the reverse runaway probability of fast electrons during current ramp-up, and a study of lower hybrid wave interaction with fusion-born alpha particles in a realistic tokamak configuration indicates that energy is transferred only from the wave to the alpha particles and no wave amplification occurs. A parameter study of ion cyclotron heating and current drive indicates that the power efficiency of minority ion current generation by IC

waves is optimized for small values of local major radius and for high electron temperatures in the studied parameter range.

Section 2 describes the generic tokamak magnetic background model used in the ASCOT code, as well as the importing of background data from experiment databases. Methods of making the evaluation of the local magnetic background computationally efficient are considered.

Section 3 gives an overview of the guiding center equations of motion and of the method of orbit-following. The accumulation of numerical error in the orbit solution and ways to alleviate it without excessive loss of computational efficiency are discussed.

In section 4, an overview of the Monte Carlo model of the particle–background interactions is given, and the approach to linking the interaction models efficiently to the orbit-following algorithm is presented. The enhancement of the computational efficiency of the code by acceleration of particle–background interaction time scales [65] is described. The implementation of this scheme and the method of determining reasonable acceleration limits are discussed.

Section 5 summarizes the applications and the results obtained in **Publications I–VI** from the point of view of the approach applied in ASCOT. Effects arising from the relativistic treatment of electrons and from the inherently modelled toroidal geometry and finite orbit widths are described.

2 The tokamak models used in ASCOT

The magnetic field lines in a tokamak wind helically around the torus, and ideally the surfaces of constant poloidal magnetic flux are perfectly nested. In the simplest tokamak model, with a circular cross section of the plasma and without the Grad–Shafranov displacement of the magnetic axis (Fig. 2a), the simplicity of the flux surface shape allows the poloidal magnetic field components to be evaluated rapidly using simple trigonometry. However, this simplified model omits many features of modern tokamaks, in which the plasma cross section is elongated and typically has some triangularity or D-shape maintained by shaping coils.

These features, as well as the Grad–Shafranov displacement of the magnetic axis (Fig. 2b) can be taken into account by relatively simple models such as the one proposed by T.E. Stringer and utilized at the JET project (see subsection 2.1). However, the computational requirements of the background model grow considerably as compared to the circular model, deteriorating the performance of any computer code that constantly needs to evaluate the local magnetic background. In a realistic tokamak configuration with a nonsymmetric cross section and an X–point (see Fig. 2c), this problem becomes even more pronounced.

The early applications of the ASCOT code (**Publications I–III**) were based

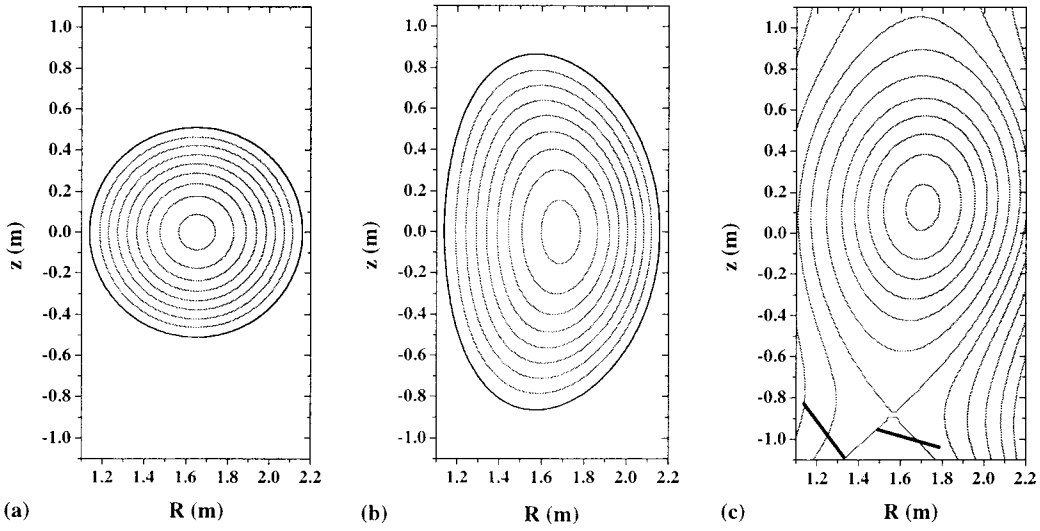

Figure 2: Tokamak plasma cross sections of different background models. a) Simple circular cross section. b) Elongated, D-shaped cross section with Grad–Shafranov displacement of the magnetic axis; only closed flux surfaces. c) Real tokamak cross section with X–point and divertor plates (ASDEX–Upgrade shot #8044 at $t = 1.32$ s.)

on the direct evaluation of the magnetic field formulas using an up-down symmetric closed flux surface model (subsection 2.1). While this approach was applicable in calculations involving only modest numbers of particles, it became apparent in the studies of **Publications IV–V** that the magnetic background model was computationally too expensive to evaluate in closed form when large particle ensembles are involved.

While it is possible to devise fast polynomial approximations of the flux surface structure and the magnetic field components of a tokamak [6], the approach adopted in the ASCOT code is to pre-tabulate the necessary magnetic variables as a function of the spatial coordinates used. During simulations, the local magnetic background is evaluated by simple, fast Lagrange interpolation from the tabulated node points. This approach offers versatility in the selection of the background model and in importing magnetic background data from experiment databases. Using this method, ASCOT evaluates the local background quantities equally fast for all the geometries shown in Fig. 2.

2.1 The symmetric closed flux surface model

As a generic model of the tokamak magnetic field, the ASCOT code uses an up-down symmetric closed flux surface model proposed by T.E. Stringer and utilized at the JET project. The model depicts realistic features such as the Grad–Shafranov displacement of the magnetic axis and the elongation and D-shape of the plasma, but does not produce X-point configurations.

The spatial coordinates R and z, R being the radial coordinate measured from the symmetry axis of the torus and z the distance from the equatorial plane, are mapped to the poloidal flux surface coordinates ρ and θ by

$$R = R_0 + \Delta(\rho) + \rho\cos\theta + D(\rho)(\cos 2\theta - 1) \quad (1)$$

$$z = \kappa\rho\sin\theta, \quad (2)$$

where R_0 is the major radius of the tokamak, $\Delta(\rho)$ is the Grad–Shafranov displacement, $D(\rho)$ is the D-shape of the flux surface ρ, and κ is the elongation of the plasma. The ρ coordinate labels a poloidal magnetic flux surface and its numerical value is defined as the half width of the surface on the equator. The poloidal angle coordinate θ increases by 2π around a flux surface; in elongated, D-shaped plasmas, it differs somewhat from the polar angle of a cylindrical coordinate system. The coordinates are shown in Fig. 3.

The plasma elongation κ is taken to be a constant, and the simple equations used in describing the Grad–Shafranov displacement Δ and the D-shape D of surface ρ are

$$\Delta(\rho) = \Delta_0 \left(1 - \frac{\rho^2}{a^2}\right) \tag{3}$$

$$D(\rho) = \frac{\delta \rho^2}{2a}\left[1 + \gamma\left(1 - \frac{\rho^2}{a^2}\right)\right], \tag{4}$$

where Δ_0 is the Grad–Shafranov displacement of the magnetic axis, a is the minor radius of the tokamak, and δ and γ are constants defining the D-shape (the constant γ defined here is not to be mixed up with the relativistic factor). Using these functions in Eqs. (1) and (2) the inverse coordinate transformation is

$$\rho^2 = \frac{a^2}{G^2}\left(\frac{a^2}{2} - AG - \sqrt{\frac{a^4}{4} - a^2 AG - \frac{G^2 z^2}{\kappa^2}}\right) \tag{5}$$

$$\theta = \arcsin\left(\frac{z}{\kappa\rho}\right), \tag{6}$$

where $A = R - R_0 - \Delta_0 + \delta z^2(1+\gamma)/a\kappa^2$ and $G = \Delta_0 - \gamma\delta z^2/a\kappa^2$.

The components of the poloidal magnetic field are obtained from

$$B_{\theta,R} = \frac{\mu_0 I(\rho)}{\pi\rho}\left(\frac{R_0}{R}\right)\frac{\sin\theta + [2D(\rho)/\rho]\sin 2\theta}{L(\rho,\theta)M(\rho)} \tag{7}$$

$$B_{\theta,z} = \frac{\mu_0 I(\rho)}{\pi\rho}\left(\frac{R_0}{R}\right)\frac{\kappa\cos\theta}{L(\rho,\theta)M(\rho)}, \tag{8}$$

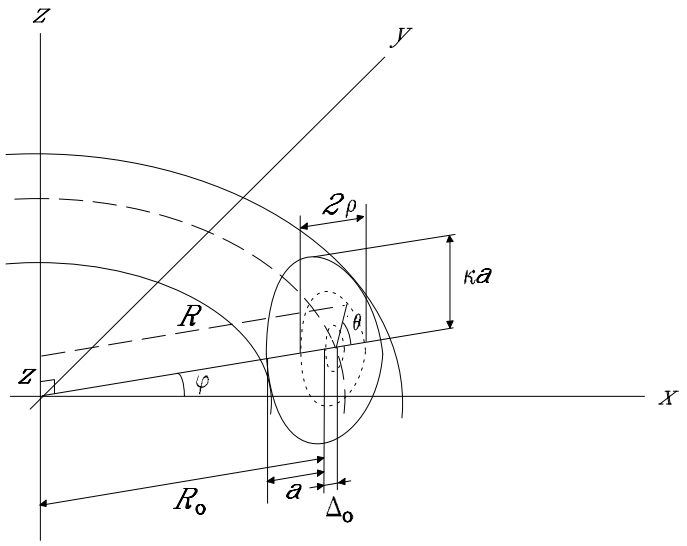

Figure 3: The coordinate system of the closed flux surface tokamak model.

where $I(\rho)$ is the total toroidal current inside the surface ρ and

$$L(\rho,\theta) = 1 + \frac{\partial\Delta(\rho)}{\partial\rho}\cos\theta \tag{9}$$

$$M(\rho) = (1+\kappa^2)\left(1-\frac{\Delta(\rho)}{R_0}\right) + \left(\frac{3\kappa^2+1}{4}\right)\left[\frac{\rho^2}{R_0^2} + \frac{\rho}{R_0}\frac{\partial\Delta(\rho)}{\partial\rho} + \left(\frac{\partial\Delta(\rho)}{\partial\rho}\right)^2\right]. \tag{10}$$

The poloidal magnetic flux ψ at the surface ρ is obtained by integrating

$$\frac{\partial\psi}{\partial R} = B_\theta R \tag{11}$$

on the equator from the magnetic axis outwards to the R value of the surface ρ.

The toroidal magnetic field is modelled with a simple 1/R dependence

$$B_\varphi = B_0\frac{R_0}{R}, \tag{12}$$

where B_0 is the toroidal magnetic field at the geometric center of the vacuum vessel.

The pressure, density and temperature profiles used with the symmetric closed flux surface model are of the form $(1-\rho^2/a^2)^g$, where the exponent g is defined by the user separately for the pressure and density profiles; the temperature profile exponent is obtained by subtracting the density profile exponent from the pressure profile exponent.

The toroidal current density profile is assumed to be flat or of the parabolic form $(1-\rho^2/a^2)$. These profiles are roughly consistent with the definitions of Δ and D. In the case of a parabolic current density profile, the total current inside the flux surface ρ is given by $I_\varphi(1-(1-\rho^2/a^2)^2)$, where I_φ is the total toroidal current.

A simple, separate computer code is used to create the magnetic background input file for the ASCOT code. The radial profiles (electron and ion density, electron and ion temperature, cross-sectional area and plasma volume) are tabulated at 21 equidistant ψ node points from the magnetic axis to the edge of the plasma, and a dense (R,z) grid of magnetic field vector (R, z, φ) components and ψ and ρ values is created, covering the whole plasma cross section. The background data are then written to a file in the format required by the ASCOT code.

2.2 Importing backgrounds from experiment databases

Importing background data from experiment databases makes it possible to study charged particle motion with as little configurational deviation from real-life measurements as possible, and thus facilitates comparisons between measurements and theoretical propositions.

As a result of the background pre-tabulation approach, the ASCOT code is readily capable of using magnetic backgrounds of real tokamaks obtained from experiment databases. With a simple computer code tailored to access the experiment database, a file is created that contains the density, temperature and magnetic background data described above in subsection 2.1 in the format required by the ASCOT code.

As a first application of a real tokamak background, the ASCOT code is being utilized in studying ion orbit–loss effects in the ASDEX Upgrade tokamak with varying plasma edge parameters. Other applications of interest are, e.g., the first wall and divertor loadings caused by superthermal particles heated by radiofrequency waves. An example of the magnetic field structure imported from the ASDEX Upgrade database is shown in Fig. 2c. For a machine of the size of ASDEX (with a major radius of 1.65 m and a minor radius of 0.5 m), an (R,z) grid of 300×300 magnetic field grid points is used.

3 Charged particle orbits in a tokamak

3.1 Charged particle motion in an electromagnetic field

The motion of a charged particle in an electromagnetic field is described by the equation of motion

$$d(m\mathbf{v})/dt = Ze(\mathbf{E} + \mathbf{v} \times \mathbf{B}), \tag{13}$$

where m is the (relativistic) mass and Z is the charge number of the particle, $\mathbf{E}$ and $\mathbf{B}$ are the electric and the magnetic field, respectively, $\mathbf{v}$ is the velocity vector of the particle, and e is the elementary charge. In a constant, uniform magnetic field the term $\mathbf{v} \times \mathbf{B}$ causes a gyration of the particle around a magnetic field line at the Larmor frequency $\Omega = ZeB/m$. The radius of the gyration (the Larmor radius) is $r_L = v_\perp/|\Omega|$, where $v_\perp$ is the particle velocity component perpendicular to the magnetic field. The presence of a constant, uniform electric field adds to the particle motion the $\mathbf{E}\times\mathbf{B}$–drift $\mathbf{v}_E = \mathbf{E} \times \mathbf{B}/B^2$ and changes the particle energy ϵ at the rate $d\epsilon/dt = Ze(\mathbf{v} \cdot \mathbf{E})$ [66]. A gradient and curvature in the magnetic field structure cause an additional drift $\mathbf{v}_{G\&C} = (v^2 + v_{||}^2)(\mathbf{B} \times \nabla B)/2\Omega B^2$, where $v_{||}$ is the velocity component to the direction of the magnetic field.

Despite the simple form of the equation of motion given above, modelling the full Larmor orbits of charged particles is computationally far too demanding in applications where it is necessary to follow the orbits of numerous particles. Even with no consideration to preventing the accumulation of numerical error, the orbit-following time step would necessarily have to be a fraction of the Larmor period $T = 2\pi/|\Omega|$, which for a hydrogen ion in a magnetic field of 1 T is of the order of $6.5 \cdot 10^{-8}$ s, and for a nonrelativistic electron as small as $3.6 \cdot 10^{-11}$ s. With the typical simulation time being of the order of 0.1...1 s per particle in most problems of interest to the test particle approach, following Larmor orbits is not feasible with present-day computing resources.

Under steady-state or slowly changing conditions in magnetic confinement plasma experiments, the guiding center approximation offers a computationally far more efficient way to describe the motion of charged particles. This model facilitates the use of time steps several orders of magnitude larger than the full orbit model.

3.2 The guiding center approximation

In a steady-state or slowly changing magnetic background of a tokamak, the magnetic field is inhomogeneous in such a manner that the field experienced by the particle over a single Larmor orbit is almost constant, i.e.,

$$\begin{aligned} \frac{r_L|\nabla B|}{B} &\ll 1 \\ \frac{1}{|\Omega|B}\frac{dB}{dt} &\ll 1. \end{aligned}$$

Under such conditions, the motion of the guiding center of the particle (i.e., the center of the Larmor gyration) can be obtained by averaging the particle velocity over the Larmor period. This yields the guiding center equation of motion [66]

$$\mathbf{v}_{gc} = \frac{v_{||}\mathbf{B}}{B} + \frac{1}{2\Omega}\frac{(v^2 + v_{||}^2)}{B^2}(\mathbf{B} \times \nabla B) + \frac{\mathbf{E} \times \mathbf{B}}{B^2}. \tag{14}$$

For orbit-following purposes, some safeguards are needed to ensure that the orbit solution does not accumulate numerical error. The constants of motion related to a charged particle moving in an electromagnetic field provide a means for monitoring the orbit solution.

The total energy of the particle in an electric field is given by

$$\epsilon = \epsilon_k + Ze\Phi, \tag{15}$$

where ϵ_k is the kinetic energy of the particle and Φ is the electric field potential. In the absence of collisions, the total energy of the particle is a constant of motion. It can be shown [66] that the magnetic moment

$$\mu = \frac{p_\perp^2}{2m_0 B} = \frac{\gamma^2 m_0 v_\perp^2}{2B}, \tag{16}$$

where γ is the relativistic factor and m_0 is the rest mass of the particle, is an adiabatic invariant for the motion of a particle in an electromagnetic field that changes slowly in space or time. For axisymmetric tokamak geometries (see Fig. 1), the toroidal canonical angular momentum P_φ, given by

$$P_\varphi = mRv_{||}B_\varphi/B + Ze\psi, \tag{17}$$

where ψ is the poloidal magnetic flux defined by Eq. 11, is a constant of motion. Expression (17) is valid for plasmas with arbitrary cross section [67]. The constants of motion given by Eqs. (15)–(17) are utilized in the orbit-following algorithm of the ASCOT code for preventing the accumulation of numerical error (see Subsection 3.5).

3.3 The coordinate systems used in ASCOT

In **Publications I–V**, the orbit-following was done using the Cartesian coordinate system (x, y, z). While applicable, this coordinate system is not optimal for use in a tokamak configuration that exhibits a helical curvature and possibly a toroidal ripple of the magnetic field lines. Unless specific preventive measures are taken (see Subsection 3.5), the orbit-following scheme is prone to accumulate numerical error.

In order to make the orbit-following scheme as accurate and efficient as possible, another coordinate system especially designed for toroidal systems, presented by A.H. Boozer [68,69], has been adopted. The Boozer coordinate system is designed specifically for toroidal systems. In this system (ψ, θ, ζ), ψ being the poloidal magnetic flux, θ a poloidal angle and ζ a toroidal angle, the helical field lines of the tokamak magnetic field are straight in the (θ, ζ) plane. The motion along the magnetic surfaces is calculated independently from the much slower drift motion perpendicular to the magnetic field lines. This makes the orbit solution less prone to numerical error accumulation, enabling the use of larger time steps or a lower-order integration routine for the equations of motion. The Boozer coordinate system is applied in **Publication VI** using the Hamiltonian equations of motion presented by White and Chance [5].

The Boozer coordinate system is used in all regions of plasma where its application is efficient and straightforward. However, in some areas, the use of the Cartesian coordinate system is required. In those regions of the tokamak where the magnetic field lines are not closed, i.e., outside the separatrix, the application of the Boozer coordinate system becomes difficult because the definition of the θ angle consistently with the region of closed flux surfaces is no longer straightforward. Another problematic region for the Boozer coordinate system is found close to the magnetic axis, where one of the variables of the White–Chance equations of motion has a singularity. As a simple solution, the Cartesian coordinate system is applied to orbit-following outside the separatrix and near the magnetic axis. In these regions, the guiding center equation of motion is given directly by Eq. (14).

In the Boozer coordinate system, the guiding center equations of motion for a tokamak configuration are given [5] by

$$\dot{\psi} = \frac{Ze}{mD}\left\{\mu_0 I\left[\frac{\partial\Phi}{\partial\zeta} + \left(\rho_{||}^2 B + \mu\right)\frac{\partial B}{\partial\zeta}\right] - g\left[\frac{\partial\Phi}{\partial\theta} + \left(\rho_{||}^2 B + \mu\right)\frac{\partial B}{\partial\theta}\right]\right\} \quad (18)$$

$$\dot{\theta} = \frac{Ze}{mD}\left\{\rho_{||} B^2\left(1 - g'\rho_{||}\right) + g\left[\frac{\partial\Phi}{\partial\psi} + \left(\rho_{||}^2 B + \mu\right)\frac{\partial B}{\partial\psi}\right]\right\} \quad (19)$$

$$\dot{\zeta} = \frac{Ze}{mD}\left\{-\mu_0 I\left[\left(\rho_{||}^2 B + \mu\right)\frac{\partial B}{\partial\psi} + \frac{\partial\Phi}{\partial\psi}\right] + \rho_{||} B^2\left(q + \mu_0 I'\rho_{||}\right)\right\} \quad (20)$$

$$\dot{\rho}_{||} = \frac{Ze}{mD}\left\{-\left(1 - g'\rho_{||}\right)\left[\left(\rho_{||}^2 B + \mu\right)\frac{\partial B}{\partial\theta} + \frac{\partial\Phi}{\partial\theta}\right] - \left(q + \mu_0 I'\rho_{||}\right)\left[\left(\rho_{||}^2 B + \mu\right)\frac{\partial B}{\partial\zeta} + \frac{\partial\Phi}{\partial\zeta}\right]\right\} \quad (21)$$

where

$$D = gq + \mu_0 I + \rho_{||}\mu_0(gI' - g'I) \quad (22)$$

and $g = B_\varphi R$, $\rho_{||} = (m/Ze)(v_{||}/B)$, $\mu = (m/Ze)^2(v_\perp^2/2B)$, $\Phi = (m/Ze)\phi$, ϕ is the potential of the radial electric field E_ψ, q is the safety factor, and $2\pi I$ is the current inside flux surface ψ. The prime is used to denote $\partial/\partial\psi$. The angle ζ is related to the toroidal φ angle by

$$\zeta = \varphi - q(\theta_p - \theta), \quad (23)$$

where

$$\theta_p = \frac{1}{q}\int_0^\theta \frac{gJ}{R^2}d\theta = \frac{g}{q}\int_0^l \frac{dl_\theta}{R|\nabla\psi|}, \quad (24)$$

and the Jacobian J is given by

$$J = \frac{\mu_0 I + gq}{g^2 + |\nabla\psi|^2}R^2 = \frac{\mu_0 I + gq}{B^2}. \quad (25)$$

In order to use the Boozer coordinate system, the ASCOT code pre-tabulates the necessary background variables into a grid of node points (ψ_i, θ_j) utilizing the

imported Cartesian (R,z) grid. The definitions for g, q and I are

$$g(\psi) = B_\varphi R \tag{26}$$

$$q(\psi) = \frac{g}{2\pi}\oint \frac{dl_\theta}{R|\nabla\psi|} \tag{27}$$

$$I(\psi) = \frac{1}{2\pi\mu_0}\oint B_\theta dl_\theta, \tag{28}$$

where the path integrals are taken along the poloidal flux surface around the magnetic axis at constant node point flux value ψ_i. The θ node point values for the needed background variable B as well as R and z (for coordinate system switching purposes) are obtained from the integral

$$\theta = \int_0^l \frac{R}{J|\nabla\psi|} dl_\theta \tag{29}$$

taken along each of the poloidal flux node surfaces ψ_i to the point where θ equals the desired node point value θ_j. The local values of B, R and z, as well as θ_p as given by Eq. (24), are stored into node point arrays at each (ψ_i,θ_j). After the tabulation of the background quantities, all partial derivatives occurring in Eqs. (18)–(22) are evaluated numerically and tabulated at the node points (ψ_i,θ_j).

3.4 Orbit-following method

The ASCOT code traces guiding center orbits of charged particles by numerically integrating the guiding center equations of motion over time steps. During a time step, the constants of motion given in Eqs. (15)–(17) are kept unchanged. The effects of a toroidal electric field, collisions and electromagnetic waves on the constants of motion are evaluated between time steps (see section 4). The time step Δt used in orbit-following is a fraction of the bounce time or transit time τ_B around the magnetic axis. It must be adequately small to allow enough steps to be taken per orbit in order to ensure the accurate reproduction of the orbit topology and to evaluate localized interactions with, e.g., RF waves without distortion of the results. However, an excessively small time step would seriously degrade the efficiency of the code. By default, the empirically selected time step $\Delta t = \tau_B/25$ is used in ASCOT.

Inside the separatrix, the Boozer coordinate system with Eqs. (18)–(21) is used to achieve the best accuracy and CPU efficiency of the orbit solution. However, the efficient use of the White–Chance equations of motion in the vicinity of the

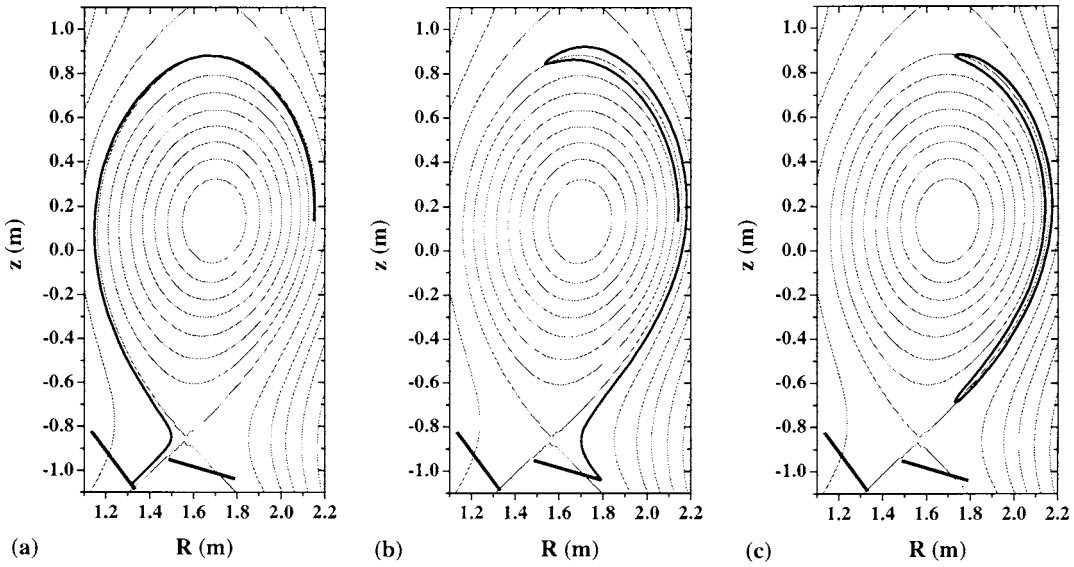

Figure 4: 5 keV deuteron orbits in the edge region of the plasma (ASDEX Upgrade shot #7934 at $t = 1.6$ s). (a) deuteron hitting the inner divertor plate. (b) deuteron hitting the outer divertor plate. (c) trapped deuteron orbit partially outside the separatrix.

magnetic axis is problematic because of the singularity of $\partial B/\partial\psi$ at the magnetic axis. Therefore, in addition to the region outside the separatrix, the Cartesian coordinate system and Eq. (14) is used when inside the ψ node point closest to the axis.

If the particle is taken over a coordinate system boundary from the region of the Boozer coordinate system to the region of the Cartesian coordinate system during a time step of orbit integration, the time step is cancelled and the integration is switched to the Cartesian coordinate system. In the opposite case, the Cartesian step is completed, after which the Boozer coordinate system is taken to use again. Using careful, accurate evaluation of the quantities related to the coordinate system change, the switching between coordinate systems at the separatrix and close to the magnetic axis has been found to work seamlessly both ways and to produce guiding center trajectories that traverse the coordinate system boundaries smoothly. Examples of orbits that cross the separatrix are shown in Fig. 4.

The integration method used in following the guiding center orbits is of crucial importance to the efficiency of the code. When following hundreds of guiding center orbits around the magnetic axis per test particle and having an ensemble of thousands of particles (as in the case of **Publication VI**), sophisticated high-

order integration methods cannot be used because of their excessive CPU time requirements. With the Boozer coordinate system of straight magnetic field lines, the simple fourth-order Runge–Kutta method without error monitoring has, in addition to being very fast, proved satisfactory in reproducing the orbit topology consistently and conserving the constants of motion in tests where large numbers of consecutive collisionless guiding center orbits were followed for test particles with varying initial parameters.

The Cartesian coordinate system, being less well suited to a toroidal geometry, gives satisfactory performance when the background is evaluated directly from the formulas of the closed flux surface tokamak model (see 2.1). With pre-tabulated, Lagrange–interpolated backgrounds, however, the Cartesian coordinate system requires the use of error monitoring, which is implemented in the ASCOT code as a part of a fifth-order Runge–Kutta scheme. The use of fifth-order integration with error monitoring reduces the speed of the code by as much as a factor of 3.

3.5 Prevention of numerical error accumulation

The numerical integration of Eq. (14) using the Cartesian coordinate system in a toroidal magnetic configuration is known [9] to be difficult and prone to accumulation of numerical error which may produce numerical drift or diffusion of the orbits. In **Publications I–III**, the accumulation of numerical error was prevented by using a hybrid integration method in which the equation of motion (14) was integrated with the fourth-order Runge–Kutta algorithm to advance the particle location $\mathbf{s}$, and after each integration step the particle location was corrected with the help of the constants of motion (15)–(17). The correction was made by solving the equations

$$(\gamma - 1)m_0c^2 = \epsilon^* \tag{30}$$

$$\gamma^2 m_0 v_\perp^2/(2B) = \mu^* \tag{31}$$

$$mRv_\parallel B_\varphi/B + Ze\psi(\rho) = P_\varphi^*, \tag{32}$$

where the quantities denoted by an asterisk refer to the values of the invariants before the integration step. The quantities on the left hand side were parametrized on a given search line $R + \alpha z = \eta$ in the poloidal plane with α and η being locally evaluated constants. The roots were searched for the set of unknowns $(v, v_\parallel, \vartheta)$, where ϑ is z or R depending on the slope of the search line.

While successful in the studies of **Publications I–III**, the procedure of separate corrections at each time step to the particle location by the constants of motion is time-consuming, with a CPU time requirement of the same order of magnitude as that of the fourth-order Runge–Kutta step. The CPU time required for a complete ASCOT run is directly proportional to the number of orbits followed per particle and the size of the test particle ensemble. As the average number of orbits followed per particle becomes larger than 100 and the size of the test particle ensemble is increased to the order of several thousands, more efficient methods of preventing error accumulation must be utilized to keep the CPU time requirement reasonable.

In **Publications IV–V**, the calculation of the guiding center velocity from Eq. (14) was modified to implicitly conserve the total energy ϵ and the toroidal momentum P_φ by using them in the calculation of the total velocity v and $v_{||}$. This approach, while leaving the exact conservation of μ unguarded, has proved satisfactory. On the other hand, this method cannot be used when toroidal magnetic field ripple is present, since P_φ is no longer conserved.

The Boozer coordinate system (see 3.3) used in **Publication VI** offers the best performance in terms of numerical accuracy and CPU efficiency. Because this coordinate system depicts the magnetic field lines as straight in the (θ, ζ) plane and motion components along and across the flux surfaces are calculated independently, the numerical integration of the equations of motion (18)–(21) has less tendency to accumulate numerical error. The constants of motion are satisfactorily conserved even without specific error monitoring in the orbit-following algorithm. However, as implemented in the ASCOT code, the Boozer coordinate system is defined only inside the separatrix where the flux surfaces are closed. The Cartesian coordinate system with error monitoring has to be used outside the separatrix in studies where test particle motion outside the plasma is of interest.

4 Particle–background interactions

In the ASCOT code, the effects of interactions between the test particle and the background are evaluated between orbit–integration time steps. The interactions affecting the velocity components and/or the radial location of the particle are evaluated using a Monte Carlo technique based on the binomial distribution. The effect of a constant toroidal electric field is taken into account by simply evaluating the change in the toroidal velocity of the particle over the orbit–integration time step Δt.

4.1 Summary of the interaction models

4.1.1 Coulomb collisions

The change in the test particle pitch $\xi = v_{||}/v$ caused by Coulomb collisions during a time step Δt is given by [4]

$$\Delta\xi = -\nu\xi\Delta t + \delta_1 \left[(1-\xi^2)\nu\Delta t\right]^{1/2}, \tag{33}$$

where ν is the pitch collision frequency and δ_1 is the evenly distributed random sign (+1 or –1) for the stochastic part of $\Delta\xi$. The operator $\Delta\xi$ has the important property of keeping the absolute value of the pitch less than one, if initially $|\xi_0| < 1$ [4].

To model the effect of Coulomb collisions on the energy of a test particle, the Monte Carlo operator given in [4] is adequate at nonrelativistic test particle energies. However, in some cases, e.g., electron studies, the relativistic effects must be taken into account. The ASCOT code uses a Monte Carlo operator derived from the linearized, relativistic Balescu–Lenard collision operator for a nonrelativistic, Maxwellian background plasma. The operator is reduced to the form of [4] at nonrelativistic energies. The effect of Coulomb collisions on the test particle energy ε is given by

$$\begin{aligned}
\Delta\varepsilon &= \Delta\varepsilon_f + \delta_2\Delta\varepsilon_s \\
&\equiv -\sum_j 2\nu_{\varepsilon,j}\Delta t\left[\varepsilon - \frac{3}{2}\gamma k_B T_j - p\frac{k_B T_j}{2}\frac{d\gamma}{dp} - \frac{1}{2}\frac{\gamma k_B T_j p}{\nu_{\varepsilon,j}}\frac{d\nu_{\varepsilon,j}}{dp}\right] \\
&\quad + \delta_2\left[\sum_j 4\gamma k_B T_j \varepsilon \nu_{\varepsilon,j}\Delta t\right]^{1/2},
\end{aligned} \tag{34}$$

where $\nu_{\varepsilon,j}$ and T_j are, respectively, the energy collision frequency and temperature for plasma species j, k_B is the Boltzmann constant, p is the (relativistic)

momentum of the test particle, δ_2 is the evenly distributed random sign (+1 or –1) for the stochastic part $\Delta\varepsilon_s$, and γ is the relativistic factor. The first term $\Delta\varepsilon_f$ in Eq. (34) is a friction term that tends to thermalize the test particle.

4.1.2 Toroidal electric field

The effect of the toroidal electric field on the particle energy during the time Δt can be written as

$$\Delta\epsilon = Ze(\mathbf{v}\cdot\mathbf{E}_\varphi)\Delta t. \tag{35}$$

In the ASCOT code, the average velocity vector during the time step Δt is used for $\mathbf{v}$ in Eq. (35). It is obtained by using the trapezoidal rule for the velocity components before and after the time step. In **Publications I–II**, this simple model was successfully benchmarked to results obtained by another method [70, 71].

4.1.3 Anomalous radial diffusion

In order to account for the effects of anomalous radial diffusion of particles on the radial distribution of absorbed radiofrequency power and driven current (**Publications II–III**), a simple Monte Carlo radial diffusion operator with a constant diffusion coefficient D is implemented in the code. The change in the radial coordinate ρ during a time step Δt is given by

$$\Delta\rho = D(\partial A/\partial\rho)\Delta t/A + \delta_3\sqrt{2D\Delta t}, \tag{36}$$

where A is the area of the flux surface and δ_3 is the evenly distributed random sign (+1 or –1) of the stochastic part.

4.1.4 Radiofrequency waves

Monte Carlo models describing interactions between test particles and radiofrequency waves have been installed in ASCOT. These models, while phenomenological by nature, are simple and fast to evaluate, which is of great importance when dealing with large particle ensembles.

In **Publication III**, the effect of lower hybrid (LH) waves on electrons is studied. The effect of the LH wave on the parallel momentum of a test electron is modelled with a Monte Carlo operator derived from the wave diffusion term of the diffusion equation for the test electron distribution using the procedure

described in [4]. The wave–particle interaction is evaluated when the parallel velocity of the particle is within the phase velocity range of the wave and the particle is inside the ρ boundaries of the wave region. The operator is given by

$$\Delta\lambda = -2(\lambda - \lambda^3)\hat{D}\Delta t \pm \sqrt{(1-\lambda^2)^2\hat{D}\Delta t}, \tag{37}$$

where

$$\lambda = \frac{p_{||} - (p_{||1} + p_{||2})/2}{(p_{||2} - p_{||1})/2}, \tag{38}$$

$$\hat{D} = \frac{2D_0}{[(p_{||2} - p_{||1})/2]^2}, \tag{39}$$

$$D_0 = \frac{\pi}{4}\frac{(Ze)^2 E_{LH}^2}{k_{LH}(v_{||2} - v_{||1})/2}, \tag{40}$$

$$E_{LH} = E_0 \exp\left\{\frac{-2(\rho - \rho_0)^2}{[(\rho_2 - \rho_1)/2]^2}\right\}, \tag{41}$$

and $\rho_0 = (\rho_1 + \rho_2)/2$. The indices 1 and 2 denote the boundaries for the LH wave in parallel velocity and momentum space $(v_{||}, p_{||})$ and in the radial coordinate ρ. E_{LH} and k_{LH} are the mean electric field and the wave number of the wave spectrum. The $v_{||}$ limits are defined as $v_{||1,2} = v_{ph} \pm v_d$, where $v_{ph} = 2\pi f_{LH}/k_{LH}$ is the phase velocity at the center of the spectrum, f_{LH} is the wave frequency and v_d determines the parallel velocity range of the wave phase velocities.

Publications IV–V study the effect of LH waves on α particles. The Monte Carlo model of the LH wave effect on a test ion is derived from the wave diffusion term of the diffusion equation for the test ion distribution by the procedure described in [4]. The Monte Carlo operators for wave–ion interaction, affecting the perpendicular energy $W_\perp$, the flux surface coordinate ρ and the toroidal momentum p_φ of the test particle, are given by

$$\Delta W_\perp = (1/s)[\partial/\partial W_\perp - (k_\eta/m\omega\Omega)\beta(\partial/\partial\rho)](sD)\Delta t \pm \sqrt{2D\Delta t} \tag{42}$$

$$\Delta\rho = -\Delta W_\perp (k_\eta/m\omega\Omega)\beta \tag{43}$$

$$\Delta p_\varphi = (k_\varphi R/\omega)\beta\Delta W_\perp. \tag{44}$$

Here, ω is the wave angular frequency, $k_\eta = k_\theta B_\varphi/B - k_\varphi B_\theta/B$ is the perpendicular component of the wavenumber projected on the magnetic surface, Ω is the Larmor frequency of the ion, $s(\rho)$ is the area of flux surface ρ, and β is given by $\beta = (1 + k_\chi v_{||}/\omega)/[(k_\eta v_{||}/\omega)(B_\theta/B_\varphi) - 1]$, where $k_\chi = k_\varphi B_\varphi/B$. The diffusion coefficient is $D = (1/2|k_\eta|)(\omega/k_\eta)^2(2eE_\eta)^2/\sqrt{v_\perp^2 - \omega^2/k_\eta^2}$.

In **Publication VI**, the interaction of test ions with ion cyclotron (IC) waves is modelled by Monte Carlo operators derived from the quasilinear diffusion model of IC heating given in [72]. The Monte Carlo operators are given by

$$\Delta v_\perp = \frac{Ze}{2m}\tau \exp(-z/l)\exp i\delta \left[E_+ J_{n-1}(\frac{k_\perp v_\perp}{\Omega}) + E_- J_{n+1}(\frac{k_\perp v_\perp}{\Omega})\right] \quad (45)$$

$$\Delta p_\varphi = \frac{k_\varphi R}{\omega}\Delta W \quad (46)$$

for the change in the minority ion perpendicular velocity $v_\perp$ and toroidal momentum $p_\varphi = mRv_{||}B_\varphi/B - Ze\psi$. Here, ΔW is the change in the particle energy, k_φ is the toroidal wave number, z is the vertical coordinate from the equatorial plane along the cyclotron resonance, l is a given exponential length for the wave amplitude decay in the vertical direction, and the phase angle δ is a random number between 0 and 2π. E_+ and E_- are the left-handed and right-handed circularly polarized electric field components of the wave, respectively, and $k_\perp$ is the perpendicular wave number of the fast magnetosonic wave. The change in $v_\perp$ is calculated when the ion passes through the IC resonance determined from the Doppler condition. This incremental change is proportional to the resonance duration time τ calculated in Ref. [9] for different orbit topologies. ΔW is calculated from the change of the total particle kinetic energy $\Delta W = \Delta(mv^2/2)$. After each pass through the resonance, $v_{||}$ is re-evaluated from the new toroidal momentum $p_\varphi^\star = p_\varphi + \Delta p_\varphi$ updated by Eq. (46); $v_{||}^\star = (p_\varphi^\star - Ze\psi)/(mRB_\varphi/B)$.

4.2 Implementation of the Monte Carlo operators

In the ASCOT code, the collision frequencies ν and $\nu_{\varepsilon,j}$ of Eqs. (33)–(34) and the local quantities related to the other Monte Carlo operators are evaluated after a successful time step for the upcoming time step Δt. If during the new time step some particle–background interaction causes an unacceptably large change in the particle parameters over Δt, the code returns to the starting point of the time step and shrinks Δt by a factor of 2. The collision frequencies and the local quantities for the other Monte Carlo operators retain their values that were calculated after the previous successful step. A schematic of the algorithm is shown in Fig. (5).

Since the calculation of the collision frequencies and the local quantities for the other Monte Carlo operators is much more cumbersome than the actual evaluation of the changes to the particle parameters as given by Eqs. (33)–(46), the procedure of evaluating the collision frequencies and other local quantities before the Runge–Kutta step, separately from the changes to the particle parameters (that may

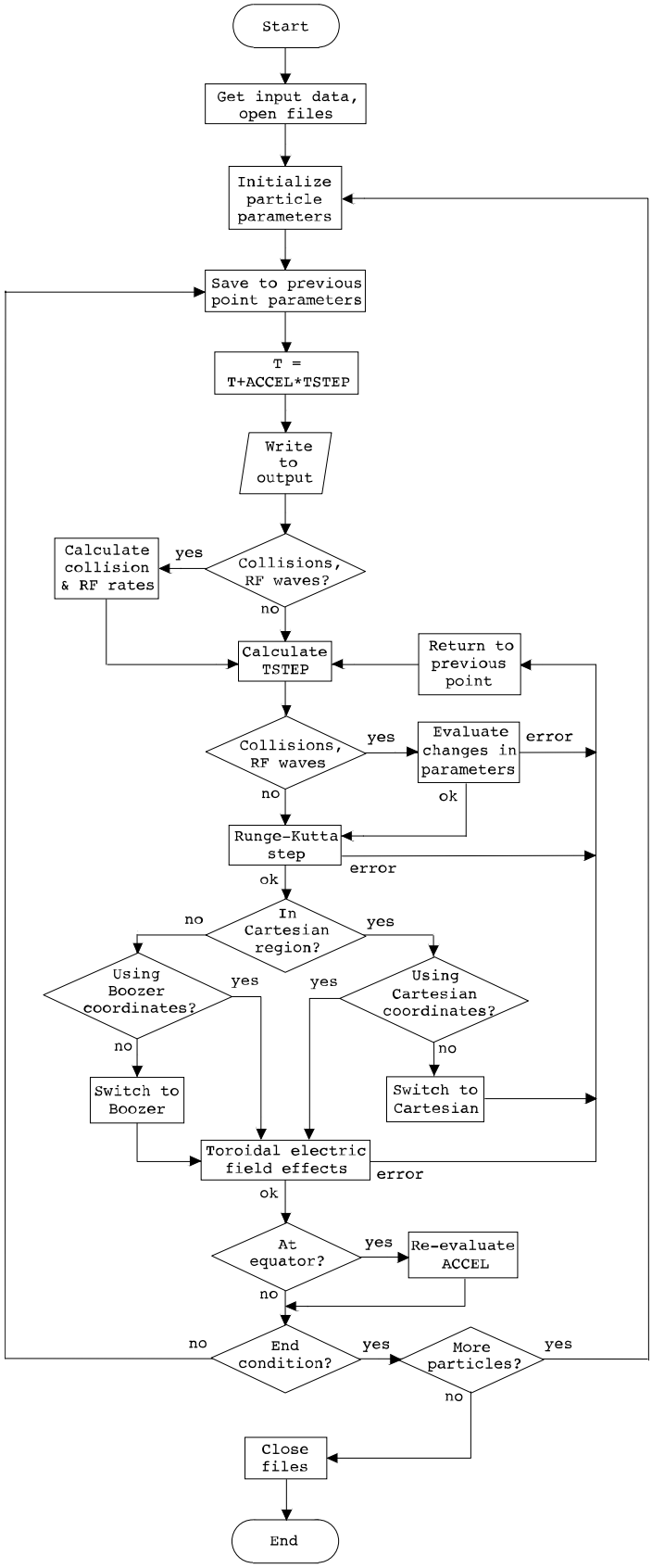

Figure 5: The flow chart of the ASCOT code.

need to be evaluated several times in case the Runge–Kutta step fails and is repeated with a smaller time step), ensures the computational efficiency of the particle–background interaction model.

4.3 Acceleration of interaction time scales

At superthermal energies, the effects of a toroidal electric field and Coulomb collisions on the test particle parameters are small per transit period around the magnetic axis. For electrons, typical collision times are in the range 1–10 ms, while the bounce time τ_B is of the order of 1 μs. Therefore, a large number of guiding center orbits must be traced in order to see significant changes in the particle parameters. An efficient way of reducing the required number of guiding center orbits per test particle is to numerically accelerate the particle–background interactions. In the ASCOT code, this is implemented by multiplying the time step Δt in the Monte Carlo operators by an acceleration factor A_{acc} determined from allowed maximal changes in particle parameters per time step or per bounce. This method is based [65] on the periodicity of the orbits in the poloidal plane when no interactions are present, and makes each followed guiding center orbit represent several orbits.

Fig. 6 shows the effect of accelerating the toroidal electric field interaction rate of an electron in the absence of collisions. In the accelerated case, the number of orbits actually followed for the test electron is dramatically reduced without significant distortion in the pitch and energy history of the electron. In terms of CPU time, the accelerated case is more than 400 times more efficient than the unaccelerated case.

In the case of radiofrequency waves, the interactions typically cause larger changes in the test particle parameters per time step. However, the time scale acceleration scheme has been found to work correctly for these interactions as well, as long as the acceleration factor is kept at a reasonable level.

The maximal relative or absolute changes in affected test particle parameters per orbit or time step are defined in the input file of the ASCOT code for each interaction separately. In the course of following the guiding center orbit, the code keeps track of the particle parameter changes caused by the various interactions that are present in the simulation. At every time step, the parameter change caused by each interaction is used to calculate a new "proposed" acceleration factor for every interaction. The smallest values of these proposed

acceleration factors are stored while the orbit is being traced. At the outermost point of each orbit, when crossing the equator of the tokamak, the smallest of the proposed acceleration factors is selected as the acceleration factor A_{acc} that is used throughout the next orbit for all interactions.

Updating the acceleration factor A_{acc} only once per orbit is important in order to keep the statistical results unbiased, since the acceleration scheme is based on the periodicity of the guiding center orbits. However, this can cause problems if the particle parameters change considerably during one guiding center orbit. For instance, the particle may experience a much stronger interaction with a radiofrequency wave than it did during the previous orbit, in which case the applied acceleration factor A_{acc}, determined from (weaker) interactions during the previous orbit, may be too large to keep the change in particle parameters

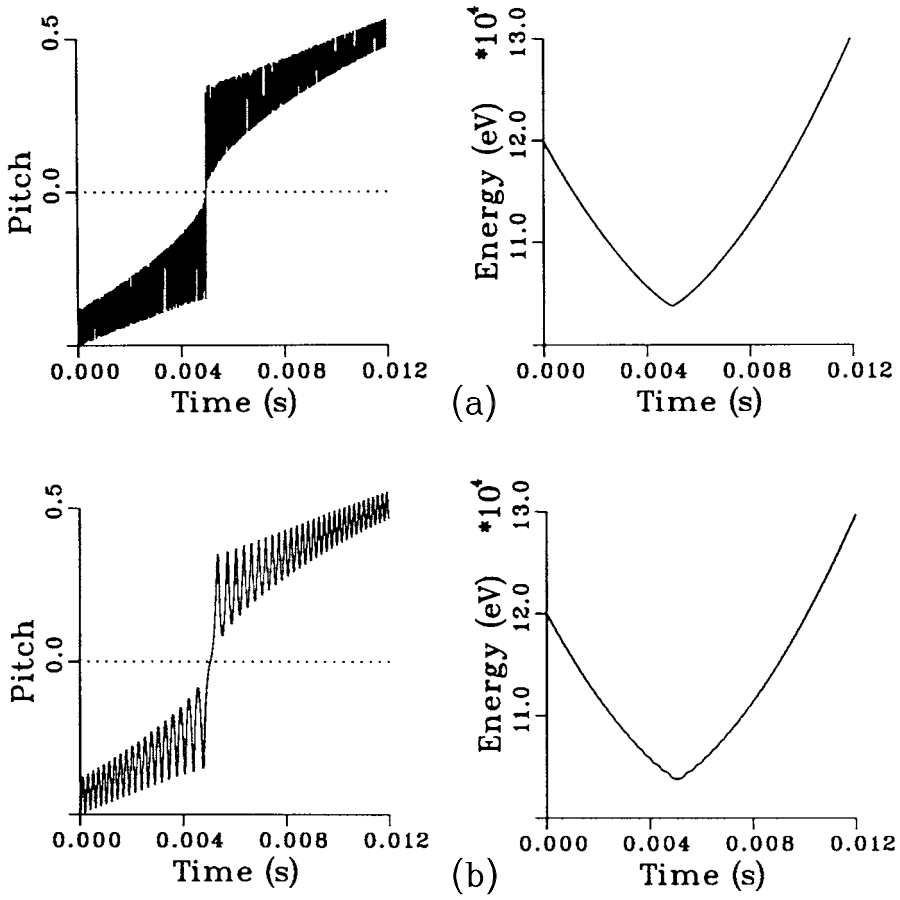

Figure 6: Effect of numerically accelerating the toroidal electric field interaction rate of an electron (no collisions). (a) Pitch and energy vs. time of a test electron in a toroidal electric field of 0.06 V/m without acceleration. (b) same as in (a), but with an average acceleration factor of 420; only about 50 orbits are calculated.

below the allowed maximum. To prevent this, a method of dividing the effect of the Monte Carlo operator into substeps of allowed magnitude has been developed for the radiofrequency operators used in **Publications IV–VI**. If the change in the test particle parameters is larger than the allowed maximum change over a time step, the Monte Carlo operator is evaluated by summing over a smaller time step Δt_i, where $\sum_i \Delta t_i = \Delta t$, so that the change in the particle parameters over each Δt_i is smaller than or equal to the allowed maximum change. The random number associated with the stochastic part of the Monte Carlo operator is re-evaluated at every substep Δt_i.

In simulations where extremely high test particle energies may be encountered, the low collisionality of the energetic particles may lead to very large acceleration factors. To avoid distortion of the statistical results, care must be taken not to allow the acceleration to reach levels where the time scale of the simulated phenomenon is reached within the order of one followed guiding center orbit. As a basic safeguard against too large acceleration factors, the ASCOT code scales the acceleration factor A_{acc} at superthermal energies by a factor $(v/v_{th})^{1/2}$, where v_{th} is the local thermal velocity [9].

The numerical acceleration of the particle–background interactions has been found to greatly enhance the efficiency of the ASCOT code. Typical acceleration factors are of the order of 100–1000 for fast particles and up to 100 for particles that are closer to thermal energy.

5 Applications of the ASCOT code

The approach of following guiding center orbits in toroidal geometry, as applied in the ASCOT code, has the advantage of inherently reproducing and taking into account realistic phenomena such as finite guiding center orbit width, trapped orbits and neoclassical radial diffusion. These are of importance when accurate estimates of particle and energy transport in tokamak geometry are required. In the following, a summary is given of the results obtained in the course of this work with an emphasis on such effects inherently modelled by ASCOT.

In the study of electron reverse runaway probability (**Publications I–II**), effects were demonstrated that are not present in simpler cylindrical models that omit finite temperature and relativistic phenomena [70, 71].

The trapping cone in $(v_{||}, v_{\perp})$ space, where the electrons have insufficient toroidal momentum to reach the equator on the inboard side of the plasma, enables the electrons to traverse a wide region in $v_{||}$ on a fast time scale on their way to the reverse runaway velocity region, causing an increase in the reverse runaway probability. This effect, caused by the magnetic field structure of the toroidal configuration, becomes stronger in the outer regions of the plasma where the trapping cone is wider.

The relativistic treatment of the equations of motion also brings forth significant effects on the reverse runaway probability. The effect of collisions with the background plasma (modelled for a relativistic test particle in a nonrelativistic Maxwellian background), while weak at relativistic energies, acts to diminish the total energy of the electrons towards thermal energy. At relativistic energies, the collisions have a lesser effect on the velocity of the test electron. Combined to the effect of pitch collisions which bring the electrons towards the trapping cone, this relativistic effect enables the electrons to reach the trapping cone at a large total velocity, where the trapping cone is wide and the $v_{||}$ region traversed during trapped orbit motion is larger. This brings forth a notable increase in the reverse runaway probability.

A finite temperature effect on the reverse runaway probability was also demonstrated. The energy diffusion becomes stronger and the slowing–down effect decreases when the temperature of the background plasma is increased. Because of this, electrons may reach the trapping cone at higher total velocity. This leads to an increase in the reverse runaway probability by making the $v_{||}$ region traversed inside the trapping cone larger.

The effect of reverse runaways on the efficiency of plasma current ramp-up by LH waves (**Publication II**) was studied in the presence of anomalous radial diffusion. In comparison to results obtained by a cylindrical model omitting finite temperature effects [71], the current ramp-up efficiency was found to deteriorate rapidly for electrons with high initial $v_{||}$. Anomalous radial diffusion was found to alleviate this phenomenon slightly by allowing reverse runaway electrons to escape confinement faster.

In the LH current drive study of **Publication III**, the effect of trapped orbits can be seen as a non-Maxwellian tail of the electron parallel velocity distribution at negative parallel velocities in addition to the strong LH–driven tail at positive parallel velocities. This is caused by trapped electrons that gain energy from the LH wave while passing the wave region at positive $v_{||}$. The increase in their $|v_{||}|$ is still present in the negative $v_{||}$ leg of the trapped orbits since the thermalizing effect of collisions is small per orbit. Also, at outer magnetic surfaces, the electrons slowing down from the $v_{||}$ region of the LH wave have a larger probability of becoming trapped before thermalization because the trapping cone is wider. These effects degrade the efficiency of LH current drive at outer magnetic surfaces since trapped particles do not contribute to the plasma current.

The studies concerning fusion-born alpha particle interaction with LH waves (**Publications IV–V**) demonstrate that the energy transfer between the alpha particles and the wave in a tokamak configuration with smooth wave diffusion and fusion reactivity profiles takes place from the wave to the particles, and no wave amplification is achieved unless a special absorbing boundary condition is applied at the perpendicular energy boundary of the wave region [73, 74]. Since the wave forces acting on an alpha particle cannot eject the particle from the wave region, the Monte Carlo operator is constructed so that the alpha particles can leave the wave perpendicular energy region only by collisional slowing-down past the wave region boundary. Wave-induced perpendicular energy changes that would eject the particle from the wave region are reflected back along the correct diffusion path in perpendicular energy and configuration space. A bidirectional current profile of alpha particles affected by the wave is observed and explained by the locally enhanced diamagnetic current density of the alpha particles [75]. The alpha particle current generation by wave momentum transfer has been evaluated and found to be affected by the wave-induced alpha particle diffusion in configuration space and by any absorbing wave region boundary conditions.

In **Publication VI**, a parameter study of plasma ion interaction with IC

waves is presented. The IC wave interaction is localized to a resonant layer at a certain value of major radius R where the Doppler resonance condition $\omega = \Omega + k_{||}v_{||}$ is fulfilled. Here, ω and Ω are the wave angular frequency and the Larmor frequency of the particle and $k_{||}$ is the parallel wave number of the IC wave. Particles with a positive $v_{||}$ interact with the wave on one side of the resonance layer and particles with a negative $v_{||}$ on the other side for a fixed sign of $k_{||}$. With finite orbit width effects in a toroidal geometry, this gives rise to a bidirectional radial profile of diamagnetic IC–heated minority ion current with a sharp gradient at the resonant layer, possibly suitable for shear modification or stabilization-related plasma current profile shaping. The bipolar minority ion current profile is produced also without a preferred direction of $k_{||}$. With a finite $k_{||}$ to one preferred direction, the negative or positive current density of the bipolar ion current profile can be enhanced by parallel momentum input [76]. The parameter study of **Publication VI** indicates that the power efficiency of minority ion current generation by IC waves is optimized for small values of R and for high electron temperatures in the studied parameter range.

6 Conclusions

In this paper, the methods and solutions utilized in the Monte Carlo guiding center orbit-following code ASCOT have been summarized. Problems and efficiency considerations in the development of a reliable and accurate orbit-following algorithm in the presence of various particle–background interactions have been addressed.

The ASCOT code has proved its applicability to a variety of problems related to the reverse runaway phenomenon and radiofrequency heating and current drive of both electrons and ions. While presently limited to modelling phenomena where a Maxwellian background plasma can be assumed, the code is capable of efficiently addressing problems concerning energetic tail minorities arising from interactions with radiofrequency waves. The modular structure of the ASCOT code makes the addition of new particle–background interactions straightforward.

In the guiding center orbit-following approach, realistic features of tokamak confinement, such as the elongation and D–shape of the plasma, the Grad–Shafranov displacement of the magnetic axis, as well as the separatrix and divertor plates, are inherently taken into account. In addition to generic tokamak models, magnetic backgrounds can be imported to the ASCOT code from experiment databases. This makes the code well suited for studies where spatially accurate estimates or comparisons with real tokamak experiments are required.

The ASCOT code combines an efficient toroidal coordinate system [5] producing accurate guiding center orbits by fast low-order numerical integration of the equations of motion inside the plasma with the conventional Cartesian coordinate system which is used outside the separatrix. While being more prone to numerical error accumulation and thus requiring a more refined integration method, the Cartesian coordinate system is only required in a small area and does not reduce the efficiency of the code substantially. With the two combined coordinate systems, spatially accurate calculations of particle losses and deposition on the vacuum chamber wall and divertor plates can be made efficiently.

The Monte Carlo approach to describing test particle collisions with a Maxwellian background plasma and interactions with radiofrequency waves such as the lower hybrid wave and the ion cyclotron wave has been enhanced with numerical time scale acceleration of the interactions, amended with a method of dividing the evaluation of the interaction into substeps where necessary to avoid excessive changes over a time step. The scheme has proved successful in studies

of radiofrequency heating and current drive, cutting the CPU time requirement at least by an order of magnitude. In problems that are well suited for interaction time scale acceleration, reductions in required CPU time can reach three orders of magnitude.

Having proved to be a versatile tool in modelling various issues of interest in tokamak fusion research, the ASCOT code is constantly under further development. A toroidal magnetic field ripple model for the study of ripple-trapped particles is being tested, and models for neutral beam injection (NBI) and simulated charge exchange (CX) diagnostics are being developed. Because of the approach of following guiding center orbits of non-interrelated test particles in a fixed Maxwellian background, the ASCOT code is ideally suited for massive parallelization. The relatively straightforward modification of the code to parallel processing of test particles will be carried out in the future.

References

[1] K. Binder, ed., *Monte Carlo Methods in Statistical Physics*, 2nd ed. (Springer, Berlin, 1986).

[2] K. Binder, ed., *Applications of the Monte Carlo Method in Statistical Physics*, 2nd ed. (Springer, Berlin, 1987).

[3] K. Tani, M. Azumi, H. Kishimoto, and S. Tamura, "Effect of Toroidal Field Ripple on Fast Ion Behavior in a Tokamak". J. Phys. Soc. Japan **50** (1981) 1726.

[4] A.H. Boozer and G. Kuo-Petravic, "Monte Carlo Evaluation of Transport Coefficients". Phys. Fluids **24** (1981) 851.

[5] R.B. White and M.S. Chance, "Hamiltonian Guiding Center Drift Orbit Calculation for Plasmas of Arbitrary Cross Section". Physics of Fluids **27** (1984) 2455.

[6] R.B. White and A.H. Boozer, "Rapid Guiding Center Calculations". Phys. Plasmas **2** (1995) 2915.

[7] G.G. Lister, "FAFNER: A Fully 3-D Neutral Beam Injection Code Using Monte Carlo Methods". Max-Planck-Institut für Plasmaphysik Report IPP 4/222, Garching 1985; A. Teubel, "FAFNER2: 3-D 'Flux Coordinate' Neutral Beam Injection Code Using Monte Carlo Methods". Max-Planck-Institut für Plasmaphysik Report IPP 4/266, Garching 1994.

[8] K. Hanatani and F.-P. Penningsfeld, "Resonant Superbanana and Resonant Banana Losses of Injected Fast Ions in Heliotron E and Wendelstein VII-A: Effects of the Radial Electric Field". Nuclear Fusion **32** (1992) 1769.

[9] M.A. Kovanen and W.G.F. Core, "HECTOR: a Code for the Study of Charged Particles in Axisymmetric Tokamak Plasmas". J. Comput. Phys. **105** (1993) 14.

[10] G.D. Porter, "A Compendium of Computer Codes for the Researcher in Magnetic Fusion Energy". Report UCID 21574-Rev.1, Lawrence Livermore National Laboratory, Livermore, CA 1989.

[11] R.T. McCann, R.J. Goldston, and D.C. McCune, "General guiding center drifts in TRANSP". Princeton Plasma Physics Laboratory Report PPPL-2684. Princeton University 1990.

[12] C.K. Birdsall and A.B. Langdon, *Plasma Physics via Computer Simulation* (McGraw-Hill, 1985).

[13] W.W. Lee and W.M. Tang, "Gyrokinetic Particle Simulation of Ion Temperature Gradient Drift Instabilities". Phys. Fluids **31** (1988) 612.

[14] G. Rewoldt and W.M. Tang, "Toroidal Microinstability Studies of High-Temperature Tokamaks". Phys. Fluids B **2** (1990) 318.

[15] R.D. Sydora, T.S. Hahm, W.W. Lee, and J.M. Dawson, "Fluctuations and Transport Due to Ion-Temperature-Gradient-Driven Instabilities". Phys. Rev. Lett. **64** (1990) 2015.

[16] X.Q. Xu and M.N. Rosenbluth, "Numerical Simulation of Ion-Temperature-Gradient-Driven Modes". Phys. Fluids B **3** (1991) 627.

[17] S.E. Parker and W.W. Lee, "A Fully Nonlinear Characteristic Method for Gyrokinetic Simulation". Phys. Fluids B **5** (1993) 77;
S.E. Parker, W.W. Lee, and R.A. Santoro, "Gyrokinetic Simulation of Ion Temperature Gradient Driven Turbulence in 3D Toroidal Geometry". Phys. Rev. Lett. **71** (1993) 2042.

[18] Z. Lin, W.M. Tang, and W.W. Lee, "Gyrokinetic Particle Simulation of Neoclassical Transport". Phys. Plasmas **2** (1995) 2975.

[19] M. Ohnishi, H. Tokunaga and J. Wakabayashi, "Loss of 3.52-MeV Alpha Particles in a Tokamak Reactor". Nuclear Fusion **16** (1976) 690.

[20] M. Ohnishi, N. Ao, and J. Wakabayashi, "Loss of Alpha Particles during Slowing-Down in an Axisymmetric Tokamak Reactor". Nuclear Fusion **18** (1978) 859.

[21] W. Bauer, K.L. Wilson, C.L. Bisson, L.G. Haggmark, and R.J. Goldston, "Alpha Transport and Blistering in Tokamaks". Nuclear Fusion **19** (1979) 93.

[22] A.V. Chankin, D.D.R. Summers, and G.M. McCracken, "The Effect of Radial Electric Field on Fast Ion Losses in Divertor Tokamaks". 1992 International Conference on Plasma Physics, Innsbruck, Austria, 29 June – 3 July 1992. Europhysics Conference Abstracts **16C**, Part II, p. II-779. European Physical Society 1992.

[23] H. Xiao, R.D. Hazeltine, and P.M. Valanju, "Ion orbit loss and the poloidal electric field in a tokamak". Physics of Plasmas **1** (1994) 3641.

[24] R.E. Potok, P.A. Politzer, and L.M. Lidsky, "Ion Thermal Conductivity in a Helical Toroid". Phys. Rev. Lett. **45** (1980) 1328.

[25] H.E. Mynick, "Verification of the Classical Theory of Helical Transport in Stellarators". Phys. Fluids **25** (1982) 325.

[26] M. Wakatani, "Neoclassical Diffusion Including Ellipticity in an l=2 Helical System". Nuclear Fusion **23** (1983) 817.

[27] W. Dommaschk, W. Lotz, and J. Nührenberg, "Monte-Carlo Simulation of Neoclassical Transport in Stellarators". Nuclear Fusion **24** (1984) 794.

[28] R.H. Fowler, J.A. Rome, and J.F. Lyon, "Monte Carlo Studies of Transport in Stellarators". Phys. Fluids **28** (1985) 338.

[29] E.R. Solano, J.A. Rome, and S.P. Hirshman, "Study of Transport in the Flexible Heliac TJ-II". Nuclear Fusion **28** (1988) 157.

[30] C.D. Beidler, W.N.G. Hitchon, D.L. Grekov, and A.A. Shishkin, "Monte Carlo Evaluation of Neoclassical Transport in Torsatrons with Different Helical Winding Laws". Nuclear Fusion **30** (1990) 405.

[31] S.L. Painter and H.J. Gardner, "Orbit Confinement and Neoclassical Transport in the H-1 Heliac". Nuclear Fusion **33** (1993) 1107.

[32] A.V. Chankin and G.M. McCracken, "Loss Ion Orbits at the Tokamak Edge". Nuclear Fusion **33** (1993) 1459.

[33] B. Gagey, Y. Lapierre, and D. Marty, "Monte Carlo Studies of Ion Cyclotron Heating in Tokamaks". *Proceedings of the 3rd Joint Varenna–Grenoble Int. Symposium on Heating in Toroidal Plasmas* (Centre d'Études Nucléaires de Grenoble, France, 1982) 361.

[34] K.W. Whang and G.J. Morales, "ICRF Heating and its Effect on Single-Particle Confinement in Tokamaks". Nucl. Fusion **23** (1983) 481.

[35] M.A. Kovanen, W.G.F. Core, and T. Hellsten, "Finite orbit effects in ICRF heated tokamak plasmas". Nuclear Fusion **32** (1992) 787.

[36] T. Hellsten, L.-G. Eriksson, and J. Carlsson, "The Influence of Finite Orbit Effects on the ICRH Power Deposition". 20th EPS Conference on Controlled Fusion and Plasma Physics, Lisbon, Portugal, 26–30 July 1993.

Europhysics Conference Abstracts **17C**, Part III, p. III-1001. European Physical Society 1993.

[37] W.G.F. Core and G.A. Cottrell, "Fast Ion Current Density Profile in a Tokamak with Symmetric Launch Ion Cyclotron Resonance Heating". Nuclear Fusion **32** (1992) 1637.

[38] T. Hellsten, J. Carlsson, and L.-G. Eriksson, "Minority Ion Cyclotron Current Drive in Tokamaks". Phys. Rev. Lett. **74** (1995) 3612.

[39] S. Murakami, M. Okamoto, N. Nakajima, M. Ohnishi, and H. Okada, "Monte Carlo Simulation Study of ICRF Minority Heating in the Large Helical Device". Nuclear Fusion **34** (1994) 913.

[40] R.H. Cohen and T.D. Rognlien, "Gradient Effects on Intense, Pulsed Electron-Cyclotron-Wave Absorption and Current Drive". Phys. Fluids B **3** (1991) 3406.

[41] C.T. Hsu and D.J. Sigmar, "Alpha-Particle Losses from Toroidicity-Induced Alfvén Eigenmodes. Part I: Phase-Space Topology of Energetic Particle Orbits in Tokamak Plasma". Physics of Fluids B **4** (1992) 1492;
D.J. Sigmar, C.T. Hsu, R. White, and C.Z. Cheng, "Alpha-Particle Losses from Toroidicity-Induced Alfvén Eigenmodes. Part II: Monte Carlo Simulations and Anomalous Alpha-Loss Processes". Physics of Fluids B **4** (1992) 1506.

[42] Y. Wu and R.B. White, "Self-Consistent Study of the Alpha-Particle-Driven Toroidicity-Induced Alfvén Eigenmode". Physics of Plasmas **1** (1994) 2733.

[43] L.C. Appel et al., "Alfvén Eigenmode Induced Energetic Particle Transport in JET". Nuclear Fusion **35** (1995) 1697.

[44] R.B. White et al., "Non-Linear Analysis of the Toroidicity Induced Alfvén Eigenmode". Nuclear Fusion **35** (1995) 1707.

[45] K. Hanatani, M. Wakatani, and K. Uo, "Monte Carlo Calculation of Perpendicular Neutral-Beam Injection in Helical Systems". Nuclear Fusion **21** (1981) 1067.

[46] R.H. Fowler, R.N. Morris, J.A. Rome, and K. Hanatani, "Neutral Beam Injection Benchmark Studies for Stellarators/Heliotrons". Nuclear Fusion **30** (1990) 997.

[47] J.G. Pérez and M. Liniers, "Theoretical Evaluations of Neutral Beam Injection Efficiency for the TJ-II Helical-Axis Stellarator". Fusion Technology **24** (1993) 251.

[48] A. Teubel and F.-P. Penningsfeld, "Collisionless Fast Ion Confinement and Computed NBI Heating Efficiency in Stellarators – a Comparative Study of W7-A, W7-AS, and W7-X". 20th European Conference on Controlled Fusion and Plasma Physics, Lisbon, Portugal, 26–30 July 1993. Europhysics Conference Abstracts **17C**, Part I, p. I-401. European Physical Society 1993.

[49] A. Teubel and F.-P. Penningsfeld, "Influence of Radial Electric Fields on the Heating Efficiency of Neutral Beam Injection in the W7-AS Stellarator". Plasma Phys. Control. Fusion **36** (1994) 143.

[50] D.L. Jassby and R.J. Goldston, "Enhanced Penetration of Neutral-Beam-Injected Ions by Vertically Asymmetric Toroidal-Field Ripple". Nuclear Fusion **16** (1976) 613.

[51] M.H. Redi et al., "Collisional Stochastic Ripple Diffusion of Alpha Particles and Beam Ions on TFTR". Nuclear Fusion **35** (1995) 1191.

[52] Y. Ikeda, K. Tobita, K. Hamamatsu, K. Ushigusa, O. Naito, and H. Ikimura, "Ripple Enhanced Banana Drift Loss at the Outboard Wall during ICRF/NBI Heating in JT-60U". Nuclear Fusion **36** (1996) 759.

[53] R.B. White et al., "Alpha Particle Loss in Tokamaks". *Plasma Physics and Controlled Nuclear Fusion Research 1988*. Nuclear Fusion Supplement 1989. Proceedings of the 12th International Conference on Plasma Physics and Controlled Nuclear Fusion Research, 12–19 October 1988, Nice, France. Paper IAEA-CN-50/D-II-4. **2** 111. IAEA, Vienna 1989.

[54] W. Lotz, P. Merkel, J. Nührenberg, and E. Strumberger, "Collisionless α-Particle Confinement in Stellarators". Plasma Phys. Control. Fusion **34** (1992) 1037.

[55] R.L. Boivin, S.J. Zweben, and R.B. White, "Study of Stochastic Toroidal Field Ripple Losses of Charged Fusion Products at the Midplane of TFTR". Nuclear Fusion **33** (1993) 449.

[56] M.H. Redi et al., "Modelling TF Ripple Loss of Alpha Particles in TFTR DT Experiments". Nuclear Fusion **35** (1995) 1509.

[57] K. Tani et al., "Burn Control of Tokamak Plasma by Toroidal Field Ripple". *Plasma Physics and Controlled Nuclear Fusion Research 1988*. Nuclear Fusion Supplement 1989. Proceedings of the 12th International Conference on Plasma Physics and Controlled Nuclear Fusion Research, 12–19 October 1988, Nice, France. Paper IAEA-CN-50/D-II-5. **2** 121. IAEA, Vienna 1989.

[58] K. Tani, T. Takizuka, and M. Azumi, "Ripple Loss of Alpha Particles in a Tokamak Reactor with a Non-Circular Plasma Cross-Section". Nuclear Fusion **33** (1993) 903.

[59] K. Tani, R. Yoshino, T. Tuda, T. Takizuka, and M. Azumi, "Ripple-Assisted Fueling in Tokamak Reactors." Fusion Technology **21** (1992) 103.

[60] K. Tobita et al., "Ripple-Trapped Loss of Neutral-Beam-Injected Fast Ions in JT-60U". Phys. Rev. Lett. **69** (1992) 3060.

[61] K. Tobita, K. Tani, T. Nishitani, K. Nagashima, and Y. Kusama, "Fast Ion Losses due to Toroidal Field Ripple in JT-60U". Nuclear Fusion **34** (1994) 1097.

[62] K. Tobita et al., "Ripple Induced Fast Ion Loss, and Related Effects in JT-60U". Nuclear Fusion **35** (1995) 1585.

[63] C.D. Beidler, W.N.G. Hitchon, and J.L. Shohet, ""Hybrid" Monte Carlo Simulation of Ripple Transport in Stellarators". J. Comput. Phys. **72** (1987) 220.

[64] W.D. D'haeseleer and C.D. Beidler, "An Efficient Physics-Based Monte Carlo Algorithm for Simulating Alpha-Particle Orbits in Tokamak Fusion-Reactor Plasmas With Toroidal-Field Ripple". Comput. Phys. Comm. **76** (1993) 1.

[65] R.J. Goldston, D.C. McCune, H.H. Towner, S.L. Davis, R.J. Hawryluk, and G.L. Schmidt, "New Techniques for Calculating Heat and Particle Source Rates due to Neutral Beam Injection in Axisymmetric Tokamaks". J. Comput. Phys. **43** (1981) 61.

[66] T.G. Northrop, *The Adiabatic Motion of Charged Particles* (Interscience, New York, 1963).

[67] L.M. Hively, G.H. Miley, and J.A. Rome, "Fast-Ion Thermalization in Non-Circular Tokamaks with Large-Banana-Width Effects". Nuclear Fusion **21** (1981) 1431.

[68] A.H. Boozer, "Guiding Center Drift Equations". Phys. Fluids **23** (1980) 904.

[69] A.H. Boozer, "Transport and Isomorphic Equilibria". Phys. Fluids **26** (1983) 496.

[70] C.F.F. Karney and N.J. Fisch, "Current in Wave-Driven Plasmas". Phys. Fluids **29** (1986) 180.

[71] N.J. Fisch and C.F.F. Karney, "Conversion of Wave Energy to Magnetic Field Energy in a Plasma Torus". Phys. Rev. Lett. **54** (1985) 897.

[72] T.A. Stix, "Fast-Wave Heating of a Two-Component Plasma". Nuclear Fusion **15** (1975) 737.

[73] N.J. Fisch and J.-M. Rax, "Current Drive by Lower Hybrid Waves in the Presence of Energetic Alpha Particles". Nuclear Fusion **32**, (1992) 549.

[74] N.J. Fisch and J.-M. Rax, "Interaction of Energetic Alpha Particles with Intense Lower Hybrid Waves". Phys. Rev. Lett. **69**, (1992) 612.

[75] J.A. Heikkinen and S.K. Sipilä, "Current Driven by Lower Hybrid Heating of Thermonuclear Alpha Particles in Tokamak Reactors". Nuclear Fusion **36** (1996) 1345.

[76] N.J. Fisch, "Current Generation by Minority-Species Heating". Nuclear Fusion **21**, (1981) 15.

Abstracts of Publications I–VI

I. Hybrid integration and acceleration techniques are used to speed up the electron guiding centre orbit calculations in a toroidal axisymmetric magnetized plasma in the presence of a dc electric field. Acceleration of the computation is introduced to bridge the gap between the two different time scales: the rapid circulations of the electron around the magnetic axis and the relatively infrequent collisions and slow response to the electric field. The constants of motion method is utilized in correcting the particle position after each guiding centre step, which makes long time steps in the integration possible. The method described is applied to the simulation of reverse runaway electrons in a tokamak plasma. It is shown that in some cases fairly large average acceleration factors (100–10000) are acceptable: the statistics for an ensemble of electrons remain correct and the transition of a single electron through the trapped orbit velocity cone is properly described. A good agreement is found with 2-D Fokker–Planck calculations in the straight cylinder approximation for a cold plasma. The finite temperature and toroidal effects on the reverse runaway rate are calculated, and the adverse effects of runaway electrons on current ramp-up in tokamaks are discussed.

II. The effects of fast electron confinement and plasma temperature on the lower-hybrid current ramp-up efficiency are investigated. The production of reverse runaways in a toroidal geometry is calculated with a Monte Carlo particle following code which includes collisions and neoclassical and relativistic effects. When anomalous fast electron diffusion in the configuration space is taken into account, the ramp-up efficiency is found to be enhanced for increasing loss rate of runaway electrons. The enhancement is in accordance with a simple analytical model which expresses the efficiency as a function of average runaway electron confinement time and the runaway fraction of current carrying electrons. Larger runaway production rate is found for the electrons orbiting on outer magnetic surfaces, because their trapping region in velocity space is wider. The runaway rate is also significantly enhanced as the thermal velocity is increased up to and above 1/6 of the runaway velocity v_R. The range of the phase velocity spectrum where the waves efficiently ramp up the current is limited by these effects below

$1.3v_R$.

III. In this paper, we present a method for noninductive current drive studies based on three-dimensional simulation of test particle orbits. A Monte Carlo momentum diffusion operator is developed to model the wave-particle interaction. The scheme can be utilized in studies of current drive efficiency as well as in examining the current density profiles caused by waves with a finite parallel wave number spectrum and a nonuniform power deposition profile in a toroidal configuration space of arbitrary shape. Calculations performed with a uniform power deposition profile of lower hybrid waves for axisymmetric magnetic configurations having different aspect ratios and poloidal cross-section shape confirm the semianalytic estimates for the current drive efficiency based on the solutions of the flux surface averaged Fokker–Planck equation for configurations with circular poloidal cross section. The consequences of the combined effect of radial diffusion, magnetic trapping and radially nonhomogeneous power deposition and background plasma parameter profiles are investigated.

IV. It is shown that the radial transport of fusion born energetic alpha particles, induced by electrostatic waves traveling in one poloidal direction, is directly connected to a net momentum of alpha particles in the toroidal direction in tokamaks. Because the momentum change is almost independent of toroidal velocity, the energy required for the momentum generation remains small on an alpha population sustained by an isotropic time-independent source. By numerical toroidal Monte Carlo calculations it is shown that the current carried by alpha particles in the presence of intense well penetrated waves can reach several mega-amperes in reactor-sized tokamaks. The obtained current can greatly exceed the neoclassical bootstrap current of the alpha particles.

V. The direction and magnitude of power and momentum exchange between fast ions and electrostatic waves in slab and toroidal systems are obtained from global Monte Carlo simulations which include the quasilinear wave-induced ion diffusion both in velocity space and through a radially localized (lower hybrid) wave structure with propagation in one preferential poloidal direction in tokamaks. The model considers a full linearized collision model, finite fast ion orbits and losses in toroidal geometry, and can properly treat

the boundary effects on the particle-wave interaction in the configuration space. For an isotropic steady ion source, reduction of wave Landau damping but no wave amplification by wave localization is found for a Gaussian wave intensity distribution in radius, irrespective of the steepness of the radial gradient of the fast ion source rate. Enhanced wave-driven fast ion current, with magnitude, direction and profile determined by the boundary conditions, net power transfer and fast ion radial transport, is found to follow from the asymmetry in the parallel wavenumber spectrum created by the finite poloidal magnetic field. In the presence of intense well-penetrated waves the current carried by fusion α particles can be controlled by the choice of the poloidal wavenumber spectrum and the total current can greatly exceed the neoclassical bootstrap current of the α particles in a reactor.

VI. The characteristics of the ion current driven by localized minority ion cyclotron heating in tokamaks in the presence of well enhanced high-energy tail are examined by fully toroidal Monte Carlo guiding-centre simulations. The contribution of the diamagnetic current to the minority current drive has been found to be of importance as it dominates the resulting fast ion current in the presence of significant toroidal trapping of RF heated minority ions, and also because it is excited even with symmetric launching, thus requiring no directivity in the antenna system. The driven currents from the simulation are compared with a functional form approximating the trapped ion contribution to the minority ion diamagnetic current in the strong heating limit. The bidirectional current profile, the dependence on wave intensity, and the increase of the current generation efficiency with electron temperature and with the inverse major radius as predicted by the Monte Carlo simulations are satisfactorily reproduced by the estimate.